Interface Limited Lithium Transport in Solid-State Batteries

Dhamodaran Santhanagopalan,[†] Danna Qian,[†] Thomas McGilvray,[†] Ziying Wang,[†] Feng Wang,[‡] Fernando Camino,[‡] Jason Graetz,[‡] Nancy Dudney,[§] and Ying Shirley Meng*,[†]

[†]Department of NanoEngineering, University of California, San Diego, 9500 Gilman Drive, La Jolla, California 92093, United States
[‡]Brookhaven National Laboratory, Upton, New York 11973, United States
[§]Materials Science and Technology Division, Oak Ridge National Laboratory, Oak Ridge, Tennessee 37830, United States

Ⓢ *Supporting Information*

ABSTRACT: Understanding the role of interfaces is important for improving the performance of all-solid-state lithium ion batteries. To study these interfaces, we present a novel approach for fabrication of electrochemically active nanobatteries using focused ion beams and their characterization by analytical electron microscopy. Morphological changes by scanning transmission electron microscopy imaging and correlated elemental concentration changes by electron energy loss spectroscopy mapping are presented. We provide first evidence of lithium accumulation at the anode/current collector (Si/Cu) and cathode/electrolyte (Li_xCoO_2/LiPON) interfaces, which can be accounted for the irreversible capacity losses. Interdiffusion of elements at the Si/LiPON interface was also witnessed with a distinct contrast layer. These results highlight that the interfaces may limit the lithium transport significantly in solid-state batteries. Fabrication of electrochemically active nanobatteries also enables in situ electron microscopy observation of electrochemical phenomena in a variety of solid-state battery chemistries.

SECTION: Energy Conversion and Storage; Energy and Charge Transport
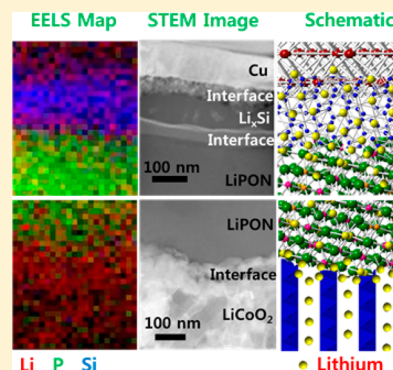
F or almost two decades, lithium ion batteries have been used heavily in consumer electronics worldwide. It is envisioned that they are potential candidates for large scale high power applications including electric vehicles. High power applications require ultrafast lithium transport between the active electrodes through electrolyte in a battery. In spite of ultrafast lithiation of isolated nanomaterials,[1−3] similar power densities have not been realized in actual devices. Such discrepancies indicate that active electrode materials alone are not responsible for the poor rate performance. There has been ample indirect evidence that both cathode and anode electrode/electrolyte interfaces can play a major role in lithium ion transport.[4,5] Nevertheless, most of the ex situ as well as in situ investigations are concentrated on the performance of either cathode or anode but not the whole system including electrolyte simultaneously.[6−9] Recently, significant interest has developed to investigate the interfaces in lithium ion batteries both theoretically[10,11] as well as experimentally.[12,13] In this respect, an all-solid-state battery is an ideal system to investigate the structural, morphological and chemical changes in the cathode, anode, electrolyte and their interfaces simultaneously. Previous attempts have not yielded promising results; nevertheless, Ruzmetov et al. investigated the scaling limits of the solid-electrolyte and claimed that it is detrimental to electrochemical performance when the electrolyte thickness is reduced down to 100 nm.[14] Yamamoto et al. investigated a solid-state battery with ultrathick electrolyte ($\sim$ 90 μm) using electron holography;[15] however, only a small portion of the battery near

the cathode/electrolyte interface was made electron transparent for their holography investigation. Brazier et al. investigated the diffusion of heavy elements across the cathode/electrolyte interface by ex situ transmission electron microscopy (TEM) and energy dispersive X-ray (EDX) analysis.[5] Despite the analysis of heavy elements, the EDX detection limit prevents lighter elements, like lithium, from being quantitatively analyzed. Along with the aforementioned characterization techniques, scanning transmission electron microscopy (STEM) coupled with electron energy loss spectroscopy (EELS) are advanced techniques to characterize structural, morphological, and chemical changes with a unique combination of high spatial, temporal resolution and chemical sensitivity. With state-of-the-art STEM/EELS, one can achieve subnanometer resolution, subsecond temporal resolution, and the detection of light elements (such as lithium) down to a few atomic percent.[16] It is equally important to minimize electron beam (e-beam) induced damages for proper quantitative measurements, which is currently lacking in the literature. Enabled with this technique, lithium concentration mapping across interfaces in nanobatteries would help with the discovery of new phenomena at the nanoscale, which may be otherwise impossible. However, direct application of STEM/EELS on all-solid-state batteries and e-beam damage quantification have not
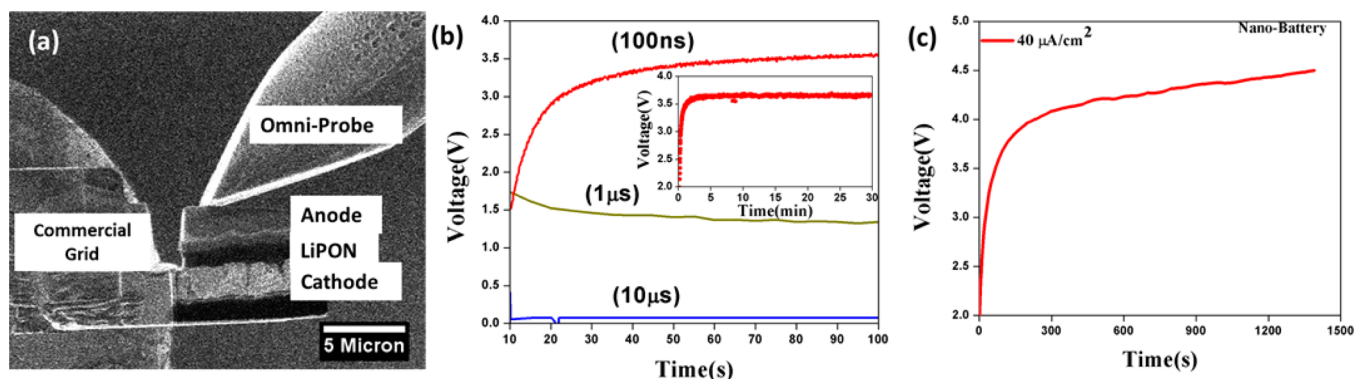
Figure 1. (a) SEM image of a typical FIB biasing of a nanobattery using an omni-probe. Electrochemical voltage profile of FIB fabricated all-solidstate. (b) Nanobattery at different fabrication pixel dwell times but fixed biasing current density of 100 $\mu A/cm^2$ and (c) nanobattery charging profile with a lower biasing current density. The inset in (b) shows 30 min charging profile of the nanobattery.

been reported in the literature to the best of our knowledge. The foremost obstacle is the difficulty in fabricating electrochemically active thin (~100 nm) all-solid-state nanobatteries. In this Letter, we elucidate the first instance of focused ion beam (FIB) fabrication of such functional all-solid-state nanobatteries and report for the first time, direct evidence of interfacial related phenomena in lithium ion batteries. Lithium accumulation at the cathode/electrolyte interface was observed during normal charging, and an additional phosphorus/silicon interdiffused layer at the electrolyte/anode interface was observed under an overcharged condition. STEM/EELS chemical mapping highlights that the cathode/electrolyte interface is the chief limiting factor for lithium transport. The current ex situ study is a crucial step in achieving in situ TEM observations of all-solid-state lithium ion batteries.

We start with an electrochemically active microbattery with Au and Cu as current collectors for the cathode ($LiCoO_2$) and anode (Si), respectively. The fabrication of such thin film batteries have been reported previously.[17−19] The optical and cross-sectional SEM images of the microbatteries used for this study are given in the Supporting Information (Figure S1). The thickness of the active layers in the current set of batteries were about 2 μm for the cathode, 1.2 μm for the electrolyte, and 80 nm for the anode. In order to study the electrochemical activity of the nanobatteries, they were biased in the FIB immediately after fabrication either using the complete isolation or the pseudoisolation scheme from the thin film battery. Both FIB biasing schemes are explained in the Supporting Information (Figure S2). The nanobatteries were charged galvanostatically (typically with a current density of about 100 $\mu A/cm^2$, equivalent to 1.25C rate) in situ in an FIB using the omniprobe as shown in Figure 1a.

First, the successful fabrication of electrochemically active nanobatteries requires very specific optimization of the FIB process, and pixel dwell time was found to be the most important factor. The charging profile for a nanobattery fabricated using a 10 μs pixel dwell time displays hardly any voltage, as shown in Figure 1b, indicating shorting across the stack, while the charging curve for a nanobattery fabricated using 1 μs pixel dwell time shows a voltage lower than the expected 3.6 V. However, when the nanobattery was fabricated using a 100 ns pixel dwell time, the charge profile shows that the voltage reaches 3.6 V. In addition, the inset in Figure 1b shows that the charging profile, when extended to 30 min (equal to 50 $\mu Ah/cm^2$), plateaus at 3.6 V throughout the entire charging period. Nanobatteries fabricated under these con-

ditions are highly consistent and repeatable with a 3.6 V voltage plateau, which agrees well with the voltage profile of microbatteries.[19] The electrochemical activity of the nanobatteries is preserved by using smaller pixel dwell time. Usage of smaller pixel dwell time is thought to minimize localized heating and compositional changes in the LiPON electrolyte, which could cause significant loss of electrochemistry. Following the successful nanobattery fabrication, we scaled down the cross-section thickness to 200 nm, and Figure 1c displays the charging profile for 40 $\mu A/cm^2$ current density. The typical current density (100 $\mu A/cm^2$), used for thicker nanobatteries was too high, leading to a large polarization, causing the voltage limit to be attained much faster in these thinner nanobatteries. Meanwhile, a 40 $\mu A/cm^2$ current density yields a profile with a plateau higher than the expected 3.6 V, indicating that the current density is still too high. As we have reached the lowest limit of our current source at 40 $\mu A/cm^2$ (using 1 pA as the absolute biasing current), we are in the process of developing a fA current source for future experiments. Cycling performance of the nanobatteries in the FIB were also investigated, and the first 10 cycles (Supporting Information, Figure S3) were similar to the microbatteries previously reported,[19] which shows a considerable amount of capacity loss.

With the developed optimized FIB process, electrochemically active nanobatteries were fabricated and then charged to different states using the pseudoisolated scheme. They were further thinned by FIB and investigated by ex situ STEM and EELS to understand the structural, morphological, and chemical changes. Results for three different samples presented here are (i) *pristine*, (ii) *charged:* to 80 $\mu Ah/cm^2$ at a rate of 1.25C, and (iii) *overcharged:* to about 260 $\mu Ah/cm^2$ at a rate of 100 times the charged sample (more details in section 2 of the Supporting Information). There are signficant morphological and chemical changes, although no detectable structural changes were found from the electron diffraction analysis within all active layers (Supporting Information, Figure S4).

As shown in Figure 2, there is a remarkable difference between the anode regions in the pristine and overcharged samples, with a sharp interface between anode and electrolyte in the former versus a broad/thick interface in the latter. The anode thickness increased significantly from 85 nm in the pristine to about 140 nm in the overcharged sample, corresponding to an expansion of about 165%, which may be due to the first stage of lithiation of amorphous silicon anodes according to the literature,[20,21] and detailed discussions are
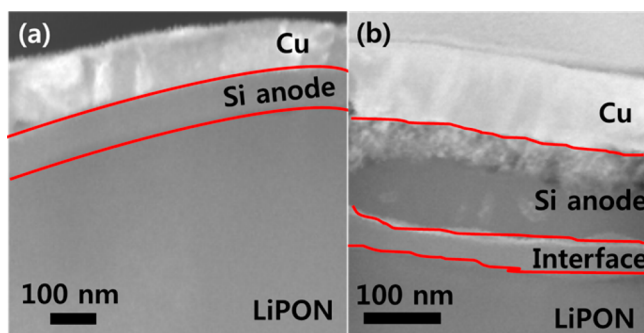
Figure 2. Cross-sectional annual dark-field STEM image of the anode region for (a) pristine and (b) overcharged samples.

given in the Supporting Information. In other cases, the different contrast in the silicon copper interface is normally attributed to the interdiffused interface upon cycling as observed by STEM/EDX analysis.[22] However, we present additional differences based on lithium concentration analysis described later in this manuscript. To correlate morphological changes with the chemical changes, EELS 2D mapping was performed on all three samples. Figure 3a−c shows the data for pristine, charged, and overcharged samples, respectively. The 2D mapping of Li, P, and Si (shown in red, green, and blue, respectively) is shown in the left image, the corresponding STEM image is in the middle, and the lithium concentration mapping is on the right. For the pristine sample, the bright red and blue regions in the cathode and anode, respectively, clearly demonstrate the pristine state of LCO and Si. The interface sharpness (as discussed above) is also clearly evidenced in these concentration maps. However, vital information can be obtained from the lithium distribution across the stack. The

variation of lithium concentration by four color gradients with increasing concentration from blue to red. For the pristine sample, lithium is concentrated in the cathode and the electrolyte while absent in the anode. In the charged and overcharged samples, the lithium has been transported to the anode, which can be seen from the green color in both cathode and anode, indicating similar concentrations of lithium in both electrodes. Actual low loss spectra from different regions of the samples are displayed in Figure S5. Interestingly, some pixels near the cathode/electrolyte interface reveals a high concentration of lithium, indicating accumulation at this interface. More detailed line scan analysis of the lithium concentration at this interface is presented in Figure 3d.

It is clearly seen that the lithium concetration is high in the cathode of pristine sample, while the charged and overcharged samples are lithium depleted. Decrease of lithium concentration near the cathode/electrolyte interface of the pristine sample was observed in several data sets, and it is possibly due to the preparation process. By contrast, an increased concentration is seen at the cathode/electrolyte interface for the charged and overcharged samples. This provides strong evidence that lithium accumulation occurs at this interface, which may play a significant role in the overall performance of the battery. The possible reason for lithium accumulation is unclear at the moment and requires more detailed study, which has been planned in the near future. The stability of active layers under e-beam during STEM/EELS are important for lithium quantification, which was performed as part of this work and reported in section 6 of the Supporting Information. Lower lithium concentration along the right edge relative to left edge of LiPON in the overcharged sample (Figure 3c) is possibly due to e-beam damage. However, due to better electronic conductivity, lithium concentration in the cathode and anode is
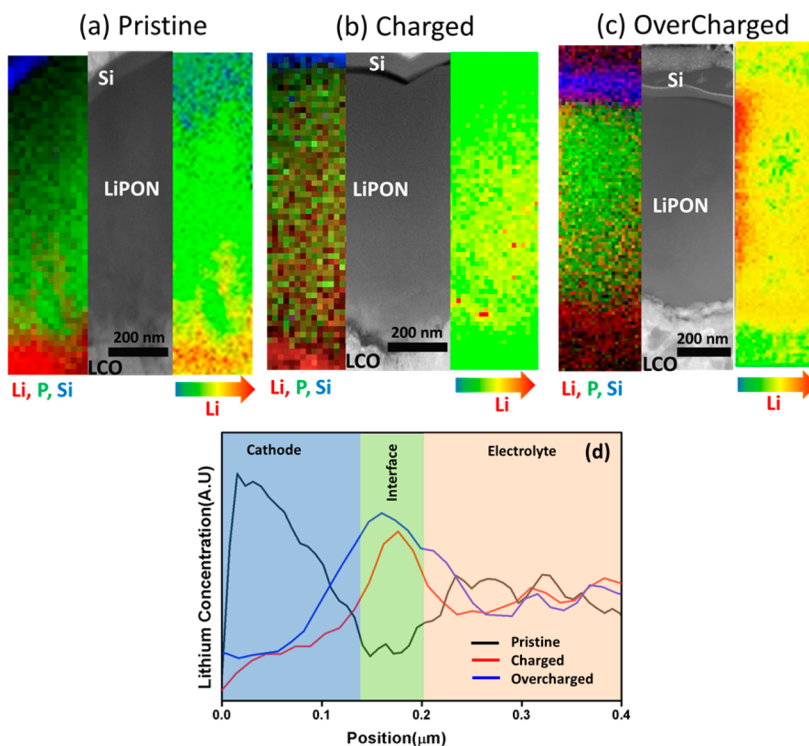

Figure 3. Elemental distribution mapped by EELS for pristine (a), charged (b), and overcharged (c) samples and lithium concentration profile (d), indicating lithium accumulation at the cathode/electrolyte interface.
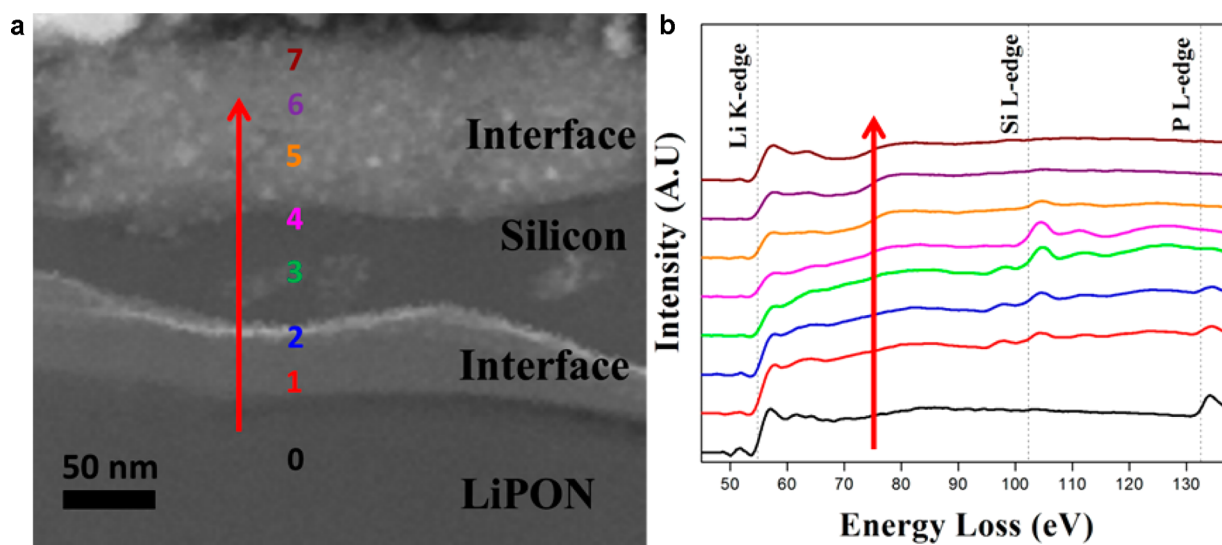
Figure 4. Annual dark-field STEM image of the anode/electrolyte interface in the overcharged sample (a) and the EELS spectra (b), recorded from 8 different sites, as labeled in the image.

not sensitive to the e-beam dose used. The results presented in this manuscript are reproducible and not heavily influenced by the lithium distribution in the LiPON layer.

Apart from lithium accumulation at the cathode/electrolyte interface, an additional anode/electrolyte interface of lithium accumulation was evident for the overcharged sample. A more detailed spectral investigation was carried out at the anode/electrolyte interface of the overcharged sample. Figure 4 displays the low-loss EELS spectra across the anode/electrolyte interface indicated by numbers "0 to 7". It is clearly seen that position 0 is from the LiPON electrolyte where Li K-edge and P L-edge peaks can be observed while the Si L-edge is not present. The spectra from positions 1 and 2 are from the interface region where all three, Li K-edge, Si L-edge and P L-edge are present. This interdiffused interface region is clearly distinct compared to the pristine sample (which exhibits a sharp interface). In the spectra from positions 3, 4, and 5, we can see that the Li K-edge and Si L-edge peaks are present, while no P L-edge is visible, indicating a lithiated silicon anode. However, spectra from positions 6 and 7 show an intense Li K-edge peak with no significant Si L-edge peak. Possibly lithium plating occurs at the Si/Cu interface, as indicated by high lithium concentration. Lithium accumulation at the silicon/metal interface has been observed recently by other groups well.[12] Additionally, lithium plating at the LiPON/Cu interface in anode-free solid-state batteries while cycling at moderate current densities have been reported previously.[23] They observed that in the absence of a protective overlayer on the copper more than 45% irreversibility at the first cycle due to lithium plating while after 100 cycles only 20% of the initial charge capacity remained. With the overlayer on copper, the capacity was retained for 1000 cycles.[23] From our set of spectral analysis, we note the formation of a phosphorus–silicon interdiffused layer in the silicon/LiPON interface upon prolonged lithiation. This interface layer shows both microscopic contrast and chemical changes. The lithium loss at the end of first cycle and subsequent cycles in solid-state batteries can be attributed to interfacial changes and lithium plating observed in the present study. Significant amount of stress due to volume expansion is possibly accommodated by the interdiffused interfaces on both sides of the anode and interface

limited reaction rate[24] as detailed in section 7 of the Supporting Information. These observations highlight that interfaces are the key limiting factor in solid-state lithium ion batteries.

To summarize, we have successfully fabricated electrochemically active all-solid-state nanobatteries for the first time and investigated the interfacial chemical changes by *semiquantitative* STEM/EELS analysis. Lithium mapping in electrochemically active nanobatteries shine light on interface-limited Li transportation across the stack. The lithium accumulation at the cathode/electrolyte interface is significant, while an additional phosphorus–silicon interdiffused anode/electrolyte interface with lithium plating at the Si/Cu interface in the overcharged sample is evidenced by both microscopic and chemical changes. More importantly, we demonstrated that crucial information on interface related issues is obtainable only through the all-solid-state battery approach. The results presented here reveal the importance of interface engineering of all-solid-state lithium ion batteries in order to improve the reversibility of lithium insertion and improve cycling and rate performances. This study also shows the viability of in situ TEM cycling of all-solid-state nanobatteries and lays the ground for exploration of new solid state chemistries at nanoscale.

■ EXPERIMENTAL METHODS

Micro all-solid-state batteries have been deposited by sputtering, and the results presented here deal with the Alumina/Pt/LiCoO$_2$/LiPON/a-Si/Cu full cell. More detailed deposition conditions are described in an earlier paper.[19] The nanobatteries (cross-sectional thickness ranging from 100 to 2000 nm, while the area was ranging from 100 μm^2 to 20 μm^2) are fabricated using FIB-SEM dual beam systems (Helios Nano Lab, FEI). The samples for (S)TEM imaging and EELS were prepared by standard FIB lift-out and thinning procedure (<80 nm thickness). Subsequent to the fabrication of nanobatteries, STEM/EELS studies are performed at 200 keV on a JEOL 2100F machine. EELS spectra were recorded in STEM mode, with a beam size of 0.5 nm, an energy resolution of about 1.1 eV, as judged by the full width at half-maximum (fwhm) of the zero-loss peak (ZLP). Lithium mapping was generated by fitting the pre-edge background using a polynomial function in the Gatan Digital Micrograph software. To avoid significant

301

dx.doi.org/10.1021/jz402467x | J. Phys. Chem. Lett. 2014, 5, 298−303

overlap with the Co M-edge, only a 5 eV window (from 52.5 to 57.5 eV) of the Li K-edge was selected for the 2D mapping. Energy window of 102 to 107 eV for Si L-edge and 132 to 137 eV for P L-edge was used to map the integrated intensity of elements.

ASSOCIATED CONTENT

ⓢ Supporting Information

We provide details about the micro- and nanobatteries, electrochemical biasing methodologies, cycling data of nanobatteries, diffraction analysis of the pristine, charged and overcharged samples, EELS lithium spectra, LiPON e-beam damage quantification, and discussion on silicon volume expansion. This material is available free of charge via the Internet at http://pubs.acs.org.

AUTHOR INFORMATION

Corresponding Author

*Mailing address: Department of NanoEngineering, University of California, San Diego, 9500 Gilman Drive, La Jolla, CA 92093. Fax: (+1) 858-534-9553; E-mail: shirleymeng@ucsd.edu.

Notes

The authors declare no competing financial interest.

ACKNOWLEDGMENTS

REFERENCES

(1) Liu, X. H.; Zhang, L. Q.; Zhong, L.; Liu, Y.; Zheng, H.; Wang, J. W.; Cho, J.-H.; Dayeh, S. A.; Picraux, S. T.; Sullivan, J. P.; et al. Ultrafast Electrochemical Lithiation of Individual Si Nanowire Anodes. *Nano Lett.* **2011**, *11*, 2251–2258.

(2) Liu, X. H.; Zheng, H.; Zhong, L.; Huang, S.; Karki, K.; Zhang, L. Q.; Liu, Y.; Kushima, A.; Liang, W. T.; Wang, J. W.; et al. Anisotropic Swelling and Fracture of Silicon Nanowires During Lithiation. *Nano Lett.* **2011**, *11*, 3312–3318.

(3) Zhang, L. Q.; Liu, X. H.; Liu, Y.; Huang, S.; Zhu, T.; Gui, L.; Mao, S. X.; Ye, Z. Z.; Wang, C. M.; Sullivan, J. P.; et al. Controlling the Lithiation-Induced Strain and Charging Rate in Nanowire Electrodes by Coating. *ACS Nano* **2011**, *6*, 4800–4809.

(4) Ohata, N.; Takada, K.; Zhang, L.; Ma, R.; Osada, M.; Sasaki, T. Enhancement of the High-Rate Capability of Solid-State Lithium Batteries by Nanoscale Interfacial Modification. *Adv. Mater.* **2006**, *18*, 2226–2229.

(5) Brazier, A.; Dupont, L.; Dantras-Laffont, L.; Kuwata, N.; Kawamura, J.; Tarascon, J. M. First Cross-Section Observation of an All Solid-State Lithium-Ion "Nanobattery" by Transmission Electron Microscopy. *Chem. Mater.* **2008**, *20* (6), 2352–2359.

(6) Wang, C. M.; Xu, W.; Liu, J.; Zhang, J. G.; Saraf, L. V.; Arey, B. W.; Choi, D.; Yang, Z. G.; Xiao, J.; Thevuthasan, S.; et al. In Situ Transmission Electron Microscopy Observation of Microstructural and Phase Evolution in a SnO_2 Nanowire during Lithium Intercalation. *Nano Lett.* **2011**, *11*, 1874–1880.

(7) Huang, J. Y.; Zhong, L.; Wang, C. M.; Sullivan, J. P.; Xu, W.; Zhang, L. Q.; Mao, S. X.; Hudak, N. S.; Liu, X. H.; Subramanian, A.; et al. In Situ Observation of the Electrochemical Lithiation of a Single SnO_2 Nanowire Electrode. *Science* **2010**, *330* (6010), 1515–1520.

(8) Yu, X.; Wang, Q.; Zhou, Y.; Li, H.; Yang, X.-Q.; Nam, K.-W.; Ehrlich, S. N.; Khalid, S.; Meng, Y. S. High Rate Delithiation Behaviour of $LiFePO_4$ Studied by Quick X-ray Absorption Spectroscopy. *Chem. Commun.* **2012**, *48*, 11537–11539.

(9) Liu, X. H.; HUang, S.; Picraux, S. T.; Li, J.; Zhu, T.; Huang, J. Y. Reversible Nanopore Formation in Ge Nanowires during Lithiation–Delithiation Cycling: An In Situ Transmission Electron Microscopy Study. *Nano Lett.* **2011**, *11*, 3991–3997.

(10) Leung, K. Electronic Structure Modeling of Electrochemical Reactions at Electrode/Electrolyte Interfaces in Lithium Ion Batteries. *J. Phys. Chem. C* **2013**, *117*, 1539–1547.

(11) Jorn, R.; Kumar, R.; Abraham, D. P.; Voth, G. A. Atomistic Modeling of the Electrode–Electrolyte Interface in Li-Ion Energy Storage Systems: Electrolyte Structuring. *J. Phys. Chem. C* **2013**, *117*, 3747–3761.

(12) Fister, T. T.; Long, B. R.; Gewirth, A. A.; Shi, B.; Assoufid, L.; Lee, S. S.; Fenter, P. Real-Time Observations of Interfacial Lithiation in a Metal Silicide Thin Film. *J. Phys. Chem. C* **2012**, *116*, 22341–22345.

(13) Carroll, K. J.; Qian, D.; Fell, C.; Calvin, S.; Veith, G. M.; Chi, M.; Baggetto, L.; Meng, Y. S. Probing the Electrode/Electrolyte Interface in the Lithium Excess Layered Oxide $Li_{1.2}Ni_{0.2}Mn_{0.6}O_2$. *Phys. Chem. Chem. Phys.* **2013**, *15*, 11128–11138.

(14) Ruzmetov, D.; Oleshko, V. P.; Haney, P. M.; Lezec, H. J.; Karki, K.; Baloch, K. H.; Agarwal, A. K.; Davydov, A. V.; Krylyuk, S.; Liu, Y.; et al. Electrolyte Stability Determines Scaling Limits for Solid-State 3D Li-Ion Batteries. *Nano Lett.* **2012**, *12*, 505–511.

(15) Yamamoto, K.; Iriyama, Y.; Asaka, T.; Hirayama, T.; Fujita, H.; Fisher, C. A. J.; Nonaka, K.; Sugita, Y.; Ogumi, Z. Dynamic Visualization of the Electric Potential in an All-Solid-State Rechargeable Lithium Battery. *Angew. Chem., Int. Ed.* **2010**, *49*, 4414–4417.

(16) Wang, F.; Yu, H. C.; Chen, M. H.; Wu, L.; Pereira, N.; Thornton, K.; Ven, A. V. D.; Zhu, Y. R.; Amatucci, G. G.; Graetz, J. Tracking Lithium Transport and Electrochemical Reactions in Nanoparticles. *Nat. Commun.* **2012**, *3*, 1201–1208.

(17) Jang, Y.-I.; Dudney, N. J.; Blom, D. A.; Allard, L. F. High-Voltage Cycling Behavior of Thin-Film $LiCoO_2$ Cathodes. *J. Electrochem. Soc.* **2002**, *149*, A1442–A1447.

(18) Yu, X.; Bates, J. B.; Jellison, G. E. J.; Hart, F. X. A Stable Thin-Film Lithium Electrolyte: Lithium Phosphorous Oxynitride. *J. Electrochem. Soc.* **1997**, *144*, 524–532.

(19) Balke, N.; Jesse, S.; Kim, Y.; Adamccky, L.; Tselev, A.; Ivanov, I. N.; Dudney, N. J.; Kalinin, S. V. Real Space Mapping of Li-Ion Transport in Amorphous Si Anodes with Nanometer Resolution. *Nano Lett.* **2010**, *10*, 3420–3425.

(20) Wang, J. W.; He, Y.; Fan, F.; Liu, X. H.; Xia, S.; Liu, Y.; Harris, C. T.; Li, H.; Huang, J. Y.; Mao, S. X.; et al. Two-Phase Electrochemical Lithiation in Amorphous Silicon. *Nano Lett.* **2013**, *13*, 709–715.

(21) McDowell, M. T.; Lee, S. W.; Harris, J. T.; Korgel, B. A.; Wang, C.; Nix, W. D.; Cui, Y. In Situ TEM of Two-Phase Lithiation of Amorphous Silicon Nanospheres. *Nano Lett.* **2013**, *13*, 758–764.

(22) Maranchi, J. P.; Hepp, A. F.; Evans, A. G.; Nuhfer, N. T.; Kumta, P. N. Interfacial Properties of the a-Si/Cu: Active-Inactive Thin-Film Anode System for Lithium-Ion Batteries. *J. Electrochem. Soc.* **2006**, *153*, A1246–A1253.

(23) Neudecker, B. J.; Dudney, N. J.; Bates, J. B. "Lithium-Free" Thin-Film Battery with In Situ Plated Li Anode. *J. Electrochem. Soc.* **2000**, *147*, 517−523.

(24) McDowell, M. T.; Ryu, I.; Lee, S. W.; Wang, C.; Nix, W. D.; Cui, Y. Studying the Kinetics of Crystalline Silicon Nanoparticle Lithiation with In Situ Transmission Electron Microscopy. *Adv. Mater.* **2012**, *24*, 6034−6041.